Variability of the Solar Angular Momentum Loss Rate Over 400 Years

Siddhant A. Deshmukh
AWESoMeStars (Supervisors: Adam Finley & Sean Matt)
Submitted: September 14, 2018

In this project, I investigated the variability of the magnetic torque on the Sun caused by the solar wind over the past 400 years. To do this, I first used measurements made by spacecraft and attempted to find a relation between the mass loss rate and the solar open flux. Then, this fitted mass loss rate was used with solar open flux from a model by Matthew Owens (University of Reading)[1] in order to determine the torque over the past 400 years (the range of the model). I found that the torque was not significantly higher than its present-day value, so the discrepancy between the predicted and calculated solar torque values are unlikely to be caused by the mass loss rate. However, it should be noted that even 400 years does not account for potential very long term variations of solar torque.

I. Introduction

It is known that main sequence stars' rotation rates slow down on the Gyr timescale[2]. This spin-down is due to the magnetic braking torque exerted on the star due to its stellar wind[]. The torque in question is due to the fact that the solar wind is magnetised and, due to the rotation of the star, it exerts a Lorentz force in a manner to counteract this rotation. This torque is dependent on the open flux and mass loss rate of the solar wind.[3]

$$\tau_w = \dot{M}_w^{1-2m} \Omega_* R_*^{2-4m} K_3^2 \left(\frac{\Phi_{open}^2}{v_{esc}(1 + f^2/K_4^2)^{1/2}} \right)^{2m} \tag{1}$$

where τ_w is the magnetic braking torque due to the solar wind, $\dot{M}_w$ is the mass loss rate due to the solar wind, Ω_* is the rotation rate of the star, R_* is the stellar radius, Φ_{open} is the open flux, v_{esc} is the escape velocity of the star and f is the fraction of breakup speed of the star. K_3, K_4 and m are parameters from simulations, and vary depending on the star in question.

For the Sun, the majority of these properties are known such that equation 1 simplifies to

$$\tau_w = 2.14 \times 10^{-7} \dot{M}^{0.26} \Phi_{open}^{1.48} \tag{2}$$

Both mass loss rate and open flux are quantities that can be derived from solar wind properties. Mass loss rate depends on the solar wind mass density and the radial wind velocity, whereas open flux depends on the radial magnetic field magnitude. I used data from 8 spacecraft (ACE, DSCOVR, WIND, Helios 1, Helios 2, STEREO A, STEREO B and Ulysses) as well as NASA/GSFC's OMNI Web service (`https://omniweb.gsfc.nasa.gov/`) which measured these and other solar wind properties. I took the hourly averages of these properties and binned them into 27-day averages to cancel out any longitudinal effects. I then attempted to fit the mass loss rate using a combination of open flux, radial wind velocity and sunspot number. I chose these parameters since they are readily available for the entire 400 year timescale.

B_r data (hence open flux data) are regularly available for the entire 400 year timescale from the model, but mass loss rate is not available for this time range. However, v_r is provided in the model along with B_r, which allows a fit for mass loss rate to be made.

II. Methods to Fit Mass Loss Rate

I used a variety of methods to constrain different parameters, but from the outset the goal was to produce a power law fit of mass loss rate. Ideally this fit would depend on parameters easily available for the 400 year timescale. I experimented with a few different fitting methods, but the main ones I used were Markov Chain Monte Carlo (MCMC) and nonlinear least squares (via the Python library scipy[4]). After generating the fits using the measurements from spacecraft, I used the functions of mass loss rate with the modelled and radial magnetic field magnitude and radial wind velocity (where applicable) over the 400 year timescale.

A. Different Fit Functions

Given that the data were very noisy and difficult to fit, I used many different functional forms to attempt the fit. These can be broken up into single variable and multi-variable fits as well, where each additional variable also added more parameters to constrain the fit further. The parameters were determined using different methods, detailed in the following subsections. To start off, I attempted to fit mass loss rate using open flux, radial wind velocity and sunspot number independently in the form

$$\dot{M} = a_1 x^{a_2} \tag{3}$$

where x is the input variable, and a_1, a_2 are the parameters of the fit. The parameters I found for all fits can be found in the appendix. From these fits, I decided to eliminate sunspot number as a primary fitting variable since it did not seem to correlate very well and produced the poorest fit. I then moved on to multi-variable fits. These were more complex and, since it increased the numbers of parameters to constrain, took longer as well. The fits were of the form

$$\dot{M} = a_1 x_1^{a_2} + a_3 x_2^{a_4} \tag{4}$$

where x_1, x_2 are different input variables and a_1, a_2, a_3, a_4 are the parameters of the fit. At this point, I ruled out sunspot number as a contributor to the fit altogether and opted to only use open flux and radial wind velocity. Trying to constrain 4 parameters also usually resulted in the algorithm attempting to eliminate v_r altogether, so I also tried normalising the variables by dividing Φ_{open} by 10^{22} and v_r by 10^{12}. This yielded slightly better results but it also seemed to be too complicated to fit. I then removed one of the coefficients and attempted a correlation of the form

$$\dot{M} = a_1 (\Phi_{open}^{a_2} + v_r^{a_3}) \tag{5}$$

This gave me the parameters $a_1 = 49.43 \pm 15.57$, $a_2 = 0.453 \pm 0.024$, $a_3 = 1.250 \pm 0.074$. I used this fit to

parametrise $\dot{M}$ in terms of Φ_{open} and v_r in order to calculate the torque from equation 2.

I also experimented with using a more complete fit of the form

$$\dot{M} = a_1 x_1^{a_2} + a_3 x_2^{a_4} + a_5 (x_1 x_2)^{a_6} \tag{6}$$

but this suffered from the same problem as trying to fit 4 parameters. I attempted it again with normalised quantities, but the fit output was identical to simply using the fit from equation 5, and so I decided to use the fit with fewer parameters.

I also tried fitting purely the crossterm, i.e.

$$\dot{M} = a_1 (\Phi_{open} v_r)^{a_2} \tag{7}$$

but this did not yield better results than equation 5.

Another fit I tried for mass loss rate was to parametrise it in terms of a mass flux; however, this gave me a worse than simply fitting mass loss rate directly and was more complicated to implement properly. The parametrisation also split v_r into the fast and slow components, with 500 [km s^{-1}] being the sharp split. then performed a fit for both the slow and fast parameters of the form

$$M = a_1 \rho v_r^{a_2} R^2 \tag{8}$$

where M is the mass flux per steradian, ρ is the mass density and R is the distance from the Sun the measurement was taken from.

B. Markov Chain Monte Carlo (MCMC) Fitting

MCMC is a procedure of sampling from a distribution via Bayesian inference, which can be used to fit parameters. Given an initial distribution for the parameters, a relation relating the independent variables and parameters to the dependent variable and an observation of the dependent variable, it constrains the parameters to best fit the function. I used the package pymc3 (`https://docs.pymc.io/`) to perform the fitting. The package has functionality to choose the number of chains for convergence; I used 10 chains as using only a couple of chains resulted in no clear fit being found.

Each parameter uses all the chains sequentially until all chains have converged, and every chain is independent from every other chain. The chain progresses from state to state, where the current state depends only on the previous state. When "scouting" for the next state, it uses a Monte Carlo process to find one and compare the viability of that state to the current state. If the posterior probability is below a certain acceptance probability, the state is accepted and the chain moves to it. Otherwise, the chain remains at the current state and searches again. Eventually, the chain will converge to the most probable value.

As the first steps are quite erratic, they are often removed (known as the burn-in period). I used a chain length of 10000 and a burn-in period of 5000 for each chain.

An alternative to using many chains could have been to massively increase the chain length, but I found that simply increasing the number of chains was sufficient for this investigation. It should also be noted that MCMC can typically only approximate the target distribution due to the residual effect of the starting position, which is another reason I chose to run multiple chains.

C. Nonlinear Least Squares

Nonlinear least squares is simply the nonlinear variant of least squares regression. It attempts to generate fits for parameters by minimising the sum of squared residuals, where the residual is just the difference between the observed data point and the modelled data point. The nonlinear case is not too dissimilar from the linear case, as it is often solved iteratively where a linear system is used as an approximation at each iteration. I used the scipy module, in particular the function "$scipy.optimize.curve\_fit()$". To fit parameters in this way, I passed in the functional form of the fit as well as the independent variables, the observed dependent variable and initial estimates of the parameters.

D. Solar Cycle Fitting

This method also used "$scipy.optimize.curve\_fit()$", but I filtered the input data to only include regions around solar minima, as the Sun is less magnetically active at this time.

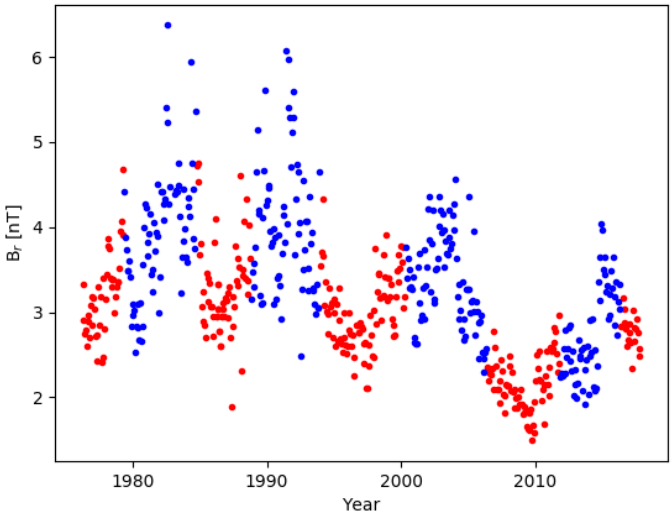

FIG. 1: Red points are chosen to be within the "minimum" and blue points are chosen to be within the "maximum."

Filtering was done by calculating the maximum and minimum values of B_r and splitting the data at the median (from minimum to maximum, then maximum to the next minimum) Then, I calculated fit parameters for a single parameter fit of the same form as equation 3. The idea was to then use the distribution of points in the "maximum" regions as a type of noise function (since the data do become more noisy at maximum due to the large increase in magnetic activity). However, I ran out of time to explore this avenue. The fit I calculated corresponded with the fits from other methods; what would set this method apart would be the noise function dependent on solar maximum data, which would give a realistic uncertainty band.

Another way to do this might be to find the relationship between B_r and v_r and try a fit from there. Again, I did not have time to explore this, but it is a viable option as Φ_{open} and $\dot{M}$ depend heavily on B_r and v_r, respectively. $\dot{M}$ also depends on solar wind mass density, though, which should be taken into account (as I did previously with a fit for mass flux).

III. Results

The distribution of mass loss rate found by the 8 individual spacecraft measurements are shown in Figure 2.

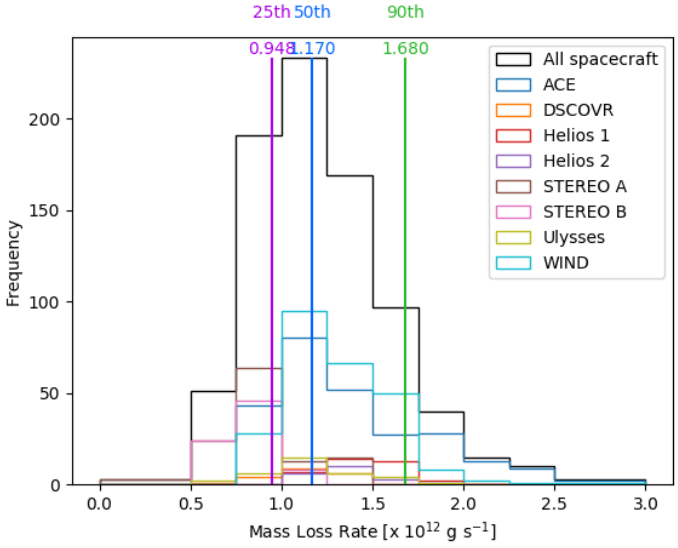

FIG. 2: Histograms of $\dot{M}$ for the 8 spacecraft whose individual measurements I used along with the overall histogram. The magenta, blue and green lines represent the 25th, 50th and 90th percentile of the overall data, respectively.

This is a distribution across the entirety of the space age and gives a limit to the bounds of mass loss rate during this time. Figure 3 shows the distribution of mass loss rate found using OMNI web service data binned by solar cycle.

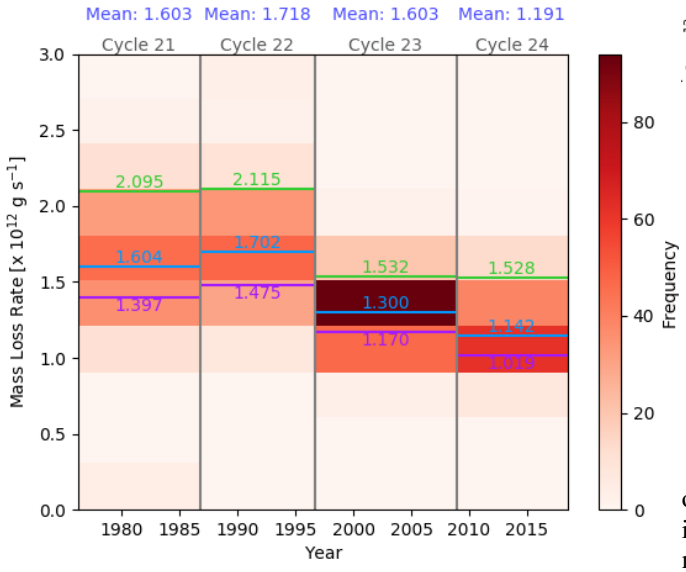

FIG. 3: Histogram of $\dot{M}$ calculated from the OMNI web service binned by solar cycle. The magenta, blue and green lines represent the 25th, 50th and 90th percentiles for each solar cycle, respectively.

Figure 4 shows the same distribution using the fitted data.

It can be seen that the model does fit the data from the space age decently well, and more importantly captures the general trend of $\dot{M}$ throughout these 4 solar cycles.

IV. Discussion

Figure 5 shows the spread of OMNI data I tried to fit, coloured by solar cycle.

It should be noted that the data from these spacecraft measurements is equatorial in nature (apart from the subset

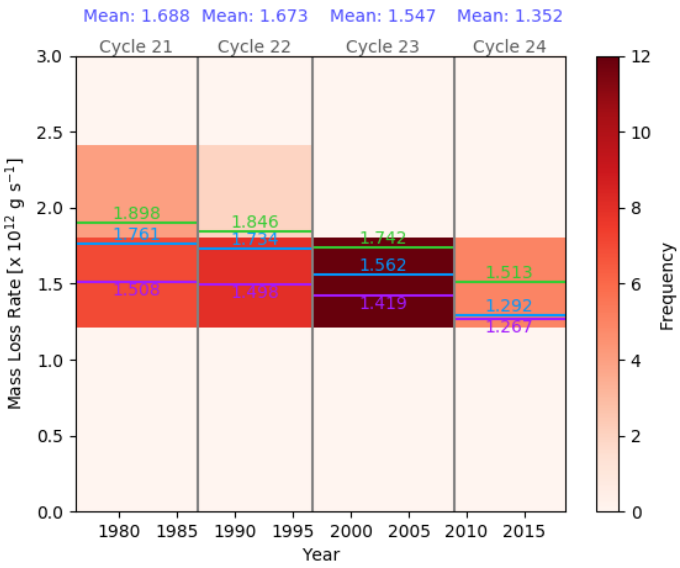

FIG. 4: Histogram of fitted $\dot{M}$ binned by solar cycle. The magenta, blue and green lines represent the 25th, 50th and 90th percentiles for each solar cycle, respectively.

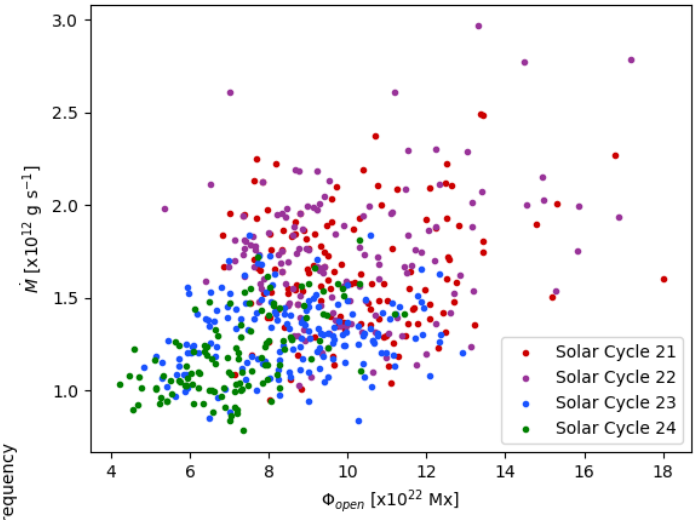

FIG. 5: Scatter of $\dot{M}$ vs. Φ_{open} for the OMNI dataset and coloured by solar cycle.

of Ulysses measurements), and therefore samples primarily the slow solar wind. The model I used gave latitudinal measurements of radial wind velocity and radial magnetic field magnitude for latitudes between $-87.5°$ and $87.5°$ at $5°$ intervals. Using purely equatorial data from this model did not seem to have a large impact on the result, as shown by figure 6.

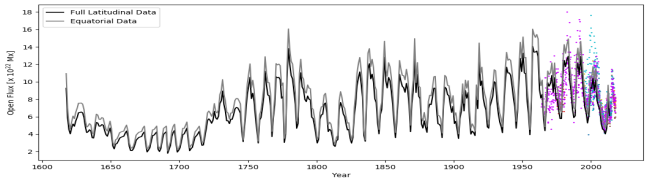

FIG. 6: Comparison of modelled open flux using the entire latitudinal data vs. just the equatorial counterpart. The points are spacecraft measuremnets.

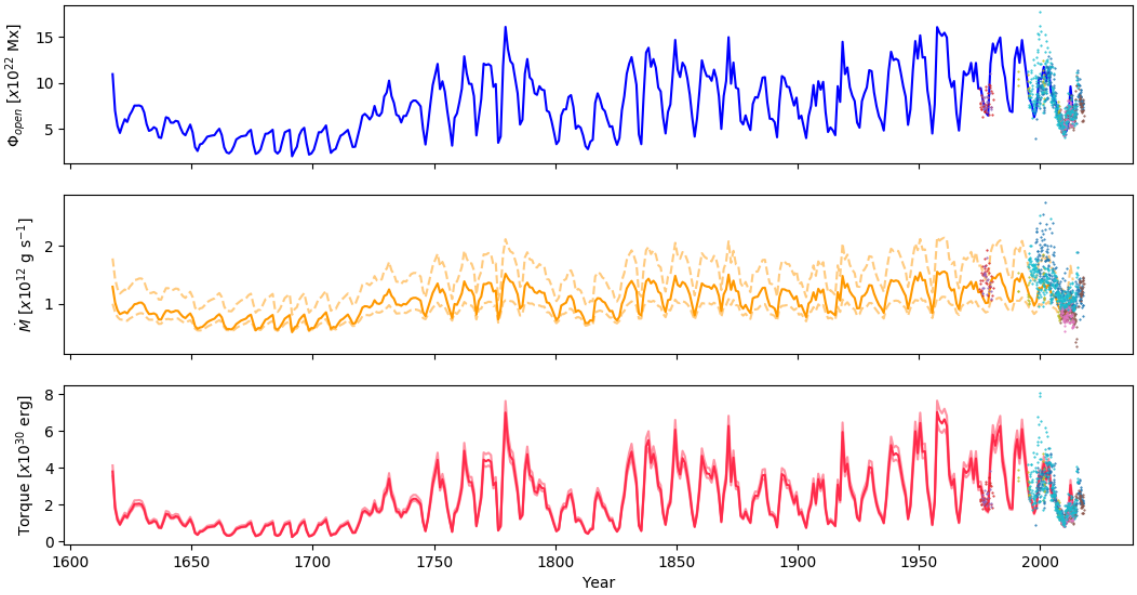

FIG. 7: From top to bottom, open flux, mass loss rate and torque variations for the last 400 years. Open flux is found from the equatorial values of B_r from the model, and mass loss rate is fitted using the MCMC method and the fit function 5. "Dispersion envelope" is shown as dashed lines in the middle panel, and as faded lines in the bottom panel.

V. Conclusions & Further Work

Figure 7 shows the open flux, mass loss rate and torque variations calculated over the 400 year timescale. A "dispersion envelope" is also plotted as a form of uncertainty. This was calculated by taking the fit, subtracting the data above and below separately, and drawing a line through the 95th percentiles of the respective differences. The line of "positive differences" (i.e. data above fit) was added to the fit to produce the upper envelope, and vice versa for the lower envelope.

I found that the solar torque over the past 400 years was not significantly high enough to account for the 3x deviation from stellar predictions. Even the highest values of $\dot{M}$ result in only a small difference to the torque, so the discrepancy is unlikely to be caused by variation in the mass loss rate. However, a 400 year timescale is still not long enough to investigate the potential variations of the solar torque on the scale of thousands or millions of years.

Additionally, using more parameters to attempt to constrain the mass loss rate did not work; though the final fit does use 3 parameters (with Φ_{open} and v_r), it is likely that the single variable Φ_{open} performs just as well.

It can be seen that due to the relatively weak dependence of torque on mass loss rate (seen from equation 2, even the fairly large dispersion in mass loss rate does not result in a large uncertainty in the torque.

To investigate longer timescales, it is possible to use cosmogenic radionuclides such as Be-10 and C-14 to reconstruct the radial magnetic field component of the solar wind. This should allow for the exploration of potentially thousands of years.

References

[1] M. J. Owens, M. Lockwood, and P. Riley. Global solar wind variations over the last four centuries. Scientific Reports, 7(January):1–11, 2017.

[2] F. Gallet and J. Bouvier. Improved angular momentum evolution model for solar-like stars. Astronomy & Astrophysics, 577:A98, 2015.

[3] Victor Réville, Allan Sacha Brun, Sean P. Matt, Antoine Strugarek, and Rui F. Pinto. The effect of magnetic topology on thermally driven wind: Toward a general formulation of the braking law. Astrophysical Journal, 798(2), 2015.

[4] Eric Jones, Travis Oliphant, Pearu Peterson, et al. SciPy: Open source scientific tools for Python, 2001–. [Online; accessed ¡today¿].

[5] H. Alfvén. On the Cosmology of the Solar System.

[6] H. Alfvén. Existence of electromagnetic-hydrodynamic waves [7]. Nature, 150(3805):405–406, 1942.

[7] Greg Balco. Contributions and unrealized potential contributions of cosmogenic-nuclide exposure dating to glacier chronology, 1990-2010. Quaternary Science Reviews, 30(1-2):3–27, 2011.

[8] Joseph E. Borovsky. On the variations of the solar wind magnetic field about the Parker spiral direction. Journal of Geophysical Research: Space Physics, 115(9):1–33, 2010.

[9] Jérôme Bouvier, Sean P. Matt, S. Mohanty, A. Scholz, K. G. Stassun, and Claudio Zanni. Angular Momentum Evolution of Young Low-Mass Stars and Brown Dwarfs: Observations and Theory. Methods and measurement in the social sciences, 1:21–32, 2010.

[10] Allan Sacha Brun and Matthew K. Browning. Magnetism, dynamo action and the solar-stellar connection. Living Reviews in Solar Physics, 14(1):4, 2017.

[11] G Corso, E Harrell, and S Paraska. Fourier Transform of the Sunspot Cycle. 71(15):1–21, 2011.

[12] Steven R. Cranmer. Why is the fast solar wind fast and the slow solar wind slow? A survey of geometrical models. European Space Agency, (Special Publication) ESA SP,

(592):159–164, 2005.

[13] Steven R. Cranmer. Mass Loss Rates from Coronal Mass Ejections: A Predictive Theoretical Model for Solar-Type Stars. The Astrophysical Journal, 840(2):114, 2017.

[14] S. T. Douglas, M. A. Agüeros, K. R. Covey, and A. Kraus. Poking the Beehive from Space: K2 Rotation Periods for Praesepe. The Astrophysical Journal, 842(2):83, 2017.

[15] Adam J. Finley and Sean P. Matt. The Effect of Combined Magnetic Geometries on Thermally Driven Winds I: Interaction of Dipolar and Quadrupolar Fields. (1967), 2017.

[16] Adam J. Finley and Sean P. Matt. The Effect of Combined Magnetic Geometries on Thermally Driven Winds II: Dipolar, Quadrupolar and Octupolar Topologies. The Astrophysical Journal, 2018.

[17] Adam J. Finley, Sean P. Matt, and Victor See. The Effect of Magnetic Variability on Stellar Angular Momentum Loss I: The Solar Wind Torque During Sunspot Cycles 23 & 24. 2018.

[18] By George E Hale. On the Probable Existence of a Magnetic Field in Sunspots. (26), 1908.

[19] M. Lockwood, M. J. Owens, and L. Barnard. Centennial variations in sunspot number, open solar flux, and streamer belt width: 2. Comparison with the geomagnetic data. Journal of Geophysical Research: Space Physics, 119(7):5183–5192, 2014.

[20] M Maksimovic, S. Peter Gary, and R M Skoug. Solar wind electron suprathermal strength and temperature gradients: Ulysses observations. Journal of Geophysical Research: Space Physics, 105(A8):18337–18350, 2000.

[21] Sean P Matt. Calculating the moment of inertia from 1-d stellar models. pages 1–2, 2017.

[22] Jennifer A Newbury, C T Russell, John L Phillips, and S Peter Gary. Electron temperature in the ambient solar wind: Typical properties and a lower bound at 1 AU. Journal of Geophysical Research, 103(A5):9553, 1998.

[23] M. J. Owens, C. N. Arge, N. U. Crooker, N. A. Schwadron, and T. S. Horbury. Estimating total heliospheric magnetic flux from single-point in situ measurements. Journal of Geophysical Research: Space Physics, 113(12):1–8, 2008.

[24] Victor Réville, Allan Sacha Brun, Antoine Strugarek, Sean P. Matt, Jérôme Bouvier, Colin P. Folsom, and Pascal Petit. FROM SOLAR to STELLAR CORONA: The ROLE of WIND, ROTATION, and MAGNETISM. Astrophysical Journal, 814(2):99, 2015.

[25] N. R. Sheeley and Y. M. Wang. THE RECENT REJUVENATION of the SUN'S LARGE-SCALE MAGNETIC FIELD: A CLUE for UNDERSTANDING PAST and FUTURE SUNSPOT CYCLES. Astrophysical Journal, 809(2):113, 2015.

[26] A. Skumanich. Time Scales for CA II Emission Decay, Rotational Braking, and Lithium Depletion. The Astrophysical Journal, 171:565, 1972.

[27] Sami K. Solanki. Sunspots: An overview. Astronomy and Astrophysics Review, 11(2-3):153–286, 2003.

[28] Sami K. Solanki, M. Schüssler, and M. Fligge. Secular variation of the Sun's magnetic flu. Astronomy & Astrophysics, 383:706–712, 2002.

[29] M. S. Venzmer and V. Bothmer. Solar-wind predictions for the Parker Solar Probe orbit. 2017.

[30] L. E. a. Vieira and S. Solanki. Evolution of the solar magnetic flux on time scales of years to millenia. 100:1–13, 2009.

[31] Y. M. Wang and N. R. Sheeley. The solar wind and interplanetary field during very low amplitude sunspot cycles. Astrophysical Journal, 764(1), 2013.

[32] Y. M. Wang and N. R. Sheeley. CORONAL MASS EJECTIONS and the SOLAR CYCLE VARIATION of the SUN'S OPEN FLUX. Astrophysical Journal Letters, 809(2):L24, 2015.

[33] Edmund J Weber and Leverett Davis. The Angular Momentum Of The Solar Wind. Astrophysical Journal, 148(April):217–227, 1967.

[34] Jeff Alstott, Ed Bullmore, and Dietmar Plenz. Powerlaw: A python package for analysis of heavy-tailed distributions. PLoS ONE, 9(1):1–18, 2014.

[35] Nicos Angelopoulos and James Cussens. Markov chain Monte Carlo using tree-based priors on model structure. Uncertainty in Artificial Intelligence: Proceedings of the Seventeenth Conference (UAI-2001), pages 16–23, 2001.

[36] A. Clauset, C. R. Shalizi, and M. E. J. Newman. POWER-LAW DISTRIBUTIONS IN EMPIRICAL DATA AARON. pages 123–132, 2009.

[37] Elan Gin, Martin Falcke, Larry E. Wagner, David I. Yule, and James Sneyd. Markov chain Monte Carlo fitting of single-channel data from inositol trisphosphate receptors. Journal of Theoretical Biology, 257(3):460–474, 2009.

[38] Elan Gin, Martin Falcke, Larry E. Wagner, David I. Yule, and James Sneyd. A kinetic model of the inositol trisphosphate receptor based on single-channel data. Biophysical Journal, 96(10):4053–4062, 2009.

[39] Elan Gin, Larry E. Wagner, David I. Yule, and James Sneyd. Inositol trisphosphate receptor and ion channel models based on single-channel data. Chaos, 19(3):1–12, 2009.

[40] David W. Hogg and Daniel Foreman-Mackey. Data analysis recipes: Using Markov Chain Monte Carlo. The Astrophysical Journal Supplement Series, 236(1):11, 2017.

Appendix: Exhaustive Results

a_1, a_2, a_3, a_4, a_5, a_6 are the fit parameters for the different mass loss rate fitting functions detailed in section II. "Single variable MCMC" and the "3 parameters, ..." fits were done using the "pymc3" package, whereas the rest were done using the "scipy" package.

Fit Method & Variables	Corresponding Equation	a_1	a_2	a_3	a_4	a_5	a_6
Single variable MCMC	3	-	-	-	-	-	-
Φ_{open} [Mx]		220.31	0.428	-	-	-	-
v_r [cm s^{-1}]		3.71×10^{10}	0.208	-	-	-	-
Sunspot Number		9.90×10^{11}	0.075	-	-	-	-
Solar Cycle Φ_{open} [Mx]	3	182.00	0.432	-	-	-	-
Crossterm, Φ_{open} [Mx], v_r [cm s^{-1}]	7	$1.187 \times 10{-}15$	0.999	-	-	-	-
Normalised Crossterm, Φ_{open} [Mx] , v_r [cm s^{-1}]	7	1.46	0.272	-	-	-	-
3 parameters, Φ_{open} [Mx], v_r [cm s^{-1}]	5	49.43	0.453	1.25	-	-	-
4 parameters, Φ_{open} [Mx], v_r [cm s^{-1}]	4	220.31	0.428	-46.72	-373.17	-	-
4 parameters, Normalised Φ_{open} [Mx], v_r [cm s^{-1}]	4	1.20	0.563	0.129	-2.32	-	-
6 parameters, Normalised Φ_{open} [Mx], v_r [cm s^{-1}]	6	4.17	0.299	-0.433	-0.433	-3.03	0.188
Mass Flux [g s^{-1}], slow wind	8	1.71×10^{-20}	5.72×10^{-13}	-	-	-	-
Mass Flux [g s^{-1}], fast wind	8	-1.74×10^{-20}	2.22×10^{-12}	-	-	-	-